Antiferromagnetic Spin Correlation of SU(N) Fermi Gas in an Optical Superlattice

Hideki Ozawa, Shintaro Taie, Yosuke Takasu, and Yoshiro Takahashi

Antiferromagnetic spin correlation of SU($\mathcal{N}$) Fermi gas in an optical super-lattice

Hideki Ozawa,* Shintaro Taie, Yosuke Takasu, and Yoshiro Takahashi

Department of Physics, Graduate School of Science, Kyoto University, Kyoto 606-8502, Japan

(Dated: November 2, 2018)

Large-spin cold atomic systems can exhibit unique phenomena that do not appear in spin-1/2 systems. We report the observation of nearest-neighbor antiferromagnetic spin correlations of a Fermi gas with SU($\mathcal{N}$) symmetry trapped in an optical lattice. The precise control of the spin degrees of freedom provided by an optical pumping technique enables us a straightforward comparison between the cases of SU(2) and SU(4). Our important finding is that the antiferromagnetic correlation is enhanced for the SU(4)-spin system compared with SU(2) as a consequence of a Pomeranchuk cooling effect. This work is an important step towards the realization of novel SU($\mathcal{N} > 2$) quantum magnetism.

Strongly correlated fermionic many-body systems play a fundamental role in modern condensed-matter physics. A central model for these systems is the Fermi-Hubbard model (FHM), originally developed for describing interacting electrons in a crystal. For a strong repulsive interaction, the two-component or SU(2) FHM is known to give rise to a paramagnetic Mott insulator at a higher temperature, whereas an antiferromagnetic order emerges below the Néel temperature [1]. In spite of intensive study for the FHM, reaching a complete understanding remained an elusive task, even for the 1/2 spin case. The development of experimental implementation of the FHM with ultracold fermionic atoms in optical lattices has provided a new approach for advancing our understanding of strongly correlated fermions [2]. The high controllability and simplicity of these systems allow systematic study over an extremely wide range of system parameters. The milestone experiments in the strongly correlated regime are recently reported realization of an antiferromagnetic correlation and order for two-component atoms in optical lattices [3–10].

While a great deal of progress has been made for two-component fermionic atoms, many body physics for multi-component fermionic atoms is hardly explored despite the theoretical interest [11–15]. Many theories have predicted that the multi-component fermionic system should exhibit rich and exotic orders at low temperatures. Fermionic isotopes of alkaline-earth-like atoms, such as ytterbium (^{173}Yb [16]) and strontium (^{87}Sr [17, 18]) in a quantum degenerate regime are suitable for this aim owing to their SU($\mathcal{N} = 2I + 1$) symmetric repulsive interactions for nuclear spin I [14, 19, 20], allowing us to access the SU($\mathcal{N} > 2$) FHM. The realization of SU(6) Mott insulating phase with ^{173}Yb ($I = 5/2$) atoms in an optical cubic lattice opens up the door of this direction of the research [21, 22]. Yet, quantum magnetism with SU($\mathcal{N}$) symmetry has not been achieved due to the required low temperature.

In this work, we measure and analyze the antiferromagnetic spin correlation of SU($\mathcal{N} = 4, 2$) Fermi gas of ^{173}Yb in an optical dimerized cubic lattice (Fig.1). This system is described by the SU($\mathcal{N}$) FHM in a dimerized lattice as

$$\hat{H}_{\mathrm{FH}} = \hat{H}_0 + \hat{H}_t, \tag{1}$$

$$\hat{H}_0 = -t_{\mathrm{d}} \sum_{\langle i,j \rangle^{\mathrm{x}}_{\underline{-}},\sigma} \left(\hat{c}^{\dagger}_{i,\sigma} \hat{c}_{j,\sigma} + \mathrm{H.c.} \right)$$

$$+ \frac{U}{2} \sum_{i,\sigma \neq \sigma'} \hat{n}_{i,\sigma} \hat{n}_{j,\sigma'} - \mu \sum_{i,\sigma} \hat{n}_{i,\sigma}, \tag{2}$$

$$\hat{H}_t = -t \sum_{\langle i,j \rangle^{\mathrm{x}}_{-},\sigma} \left(\hat{c}^{\dagger}_{i,\sigma} \hat{c}_{j,\sigma} + \mathrm{H.c.} \right)$$

$$- t_{\mathrm{yz}} \sum_{\langle i,j \rangle^{\mathrm{yz}}_{-},\sigma} \left(\hat{c}^{\dagger}_{i,\sigma} \hat{c}_{j,\sigma} + \mathrm{H.c.} \right), \tag{3}$$

where $\hat{c}_{i,\sigma}$ is the fermionic annihilation operator for a site i and spin σ, $\hat{n}_{i,\sigma} = \hat{c}^{\dagger}_{i,\sigma} \hat{c}_{i,\sigma}$ is the number operator, U is the on-site interaction energy, μ is the chemical potential, and t_d, t, t_{yz} are the tunneling amplitudes between the nearest neighbors in the strong link $\langle i,j \rangle^{\mathrm{x}}_{\underline{-}}$, the weak link $\langle i,j \rangle^{\mathrm{x}}_{-}$ along the x axis, and the weak link $\langle i,j \rangle^{\mathrm{yz}}_{-}$ along the other two axes, respectively. To reach the regime of quantum magnetism, we strongly dimerize the cubic lattice along the x direction, where the exchange interaction energy within the dimer is enhanced. As a result, we observe an excess of singlets compared with triplets. By developing a technique for optically inducing a singlet-triplet oscillation (STO) [23] with an effectively produced spin-dependent gradient, the realization of the antiferromagnetic correlation is confirmed. We investigate the spin correlation of the SU(4) system in comparison with SU(2) over a wide range of entropy. This work demonstrates the important role of large spin degrees of freedom on the quantum magnetism.

We begin with describing our experimental setup. A sample is prepared by loading an evaporatively cooled two- or four-component Fermi gas of ^{173}Yb into an optical superlattice with a dimerized cubic geometry. Our
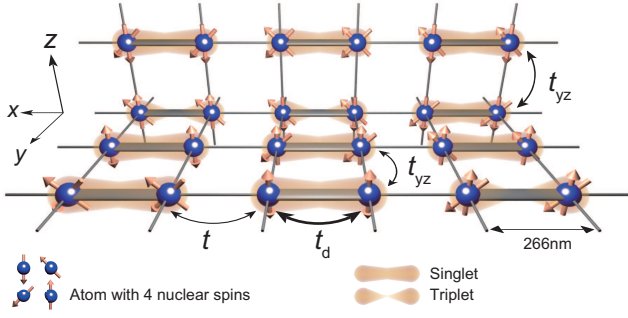
FIG. 1. Schematic view of the nearest-neighbor spin correlations in a four-component mixture of fermionic atoms prepared in a dimerized cubic lattice with the strong intra-dimer tunneling t_d and weak inter-dimer tunnelings t, t_{yz}.
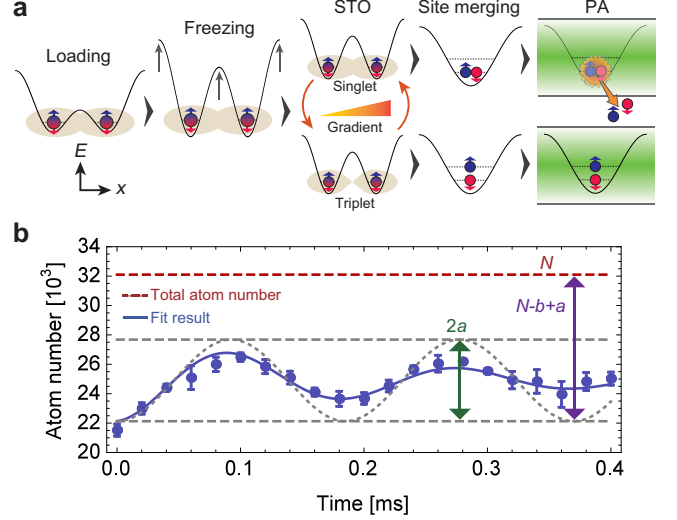

FIG. 2. (a) Detection sequence for singlets and triplets in a dimer. Shown is the case of two spins (red and blue) per dimer. Depending on the STO time, the two spins form the double occupancy in the lowest band (top), or the state with one spin in the lowest band and the other in the first excited band (bottom) after merging the dimer. These states are distinguished by the PA. (b) Singlet-triplet oscillation in a strongly dimerized lattice for SU(4) spins. The red dashed line represents the total atom number in the lattice without applying the PA. The blue solid line is the fit result with Eq.(5). The gray dotted line is the STO signal assuming no damping. Error bars denote the standard deviation of four independent scans.

optical dimerized lattice potential is given by

$$V(x, y, z) = -V_{\text{short}}^{(x)}\cos^2(2k_{\text{L}}x + \pi/2) - V_{\text{long}}^{(x)}\cos^2(k_{\text{L}}x)$$
$$-V_{\text{short}}^{(y)}\cos^2(2k_{\text{L}}y) - V_{\text{short}}^{(z)}\cos^2(2k_{\text{L}}z), \quad (4)$$

where $k_{\text{L}} = 2\pi/\lambda$ is a wave number of a long lattice, for which we choose $\lambda = 1064$ nm. The short term stability of the relative phase between short and long lattices along x-axis is $\pm 0.001\pi$ according to the relative laser linewidth. The typical phase drift is $\pm 0.01\pi$ per day. All measurements of sequential data set were finished within 1 hour of the last phase calibration. In the following, we specify each lattice depth as $s_{\text{L}} = [(s_{\text{long}}^x, s_{\text{short}}^x), s_{\text{short}}^y, s_{\text{short}}^z] = [(V_{\text{long}}^{(x)}, V_{\text{short}}^{(x)}), V_{\text{short}}^{(y)}, V_{\text{short}}^{(z)}]/E_{\text{R}}$, where $E_{\text{R}} = \hbar^2 k_{\text{L}}^2/(2m)^2$ is the recoil energy for the long lattice. Unless mentioned, atoms are initially loaded into the lattice depth of $s_{\text{L}} = [(20, 20.8), 48, 48]$, which corresponds to the Hubbard parameters of $U/h = 3.0$ kHz, $t_d/h = 1.0$ kHz, $t/h = 37$ Hz, and $t_{yz}/t = 1.3$. The tunnelings along the dimerized lattice are determined by fitting a tight-binding model to the bands of the first principle calculation. For the on-site interaction, we constructed the Wannier function with the method described in Ref.[24]. We also estimated the beyond-Hubbard terms such as nearest-neighbor interaction and density-induced tunneling [25]. They do not play an important role in our experiments.

At the early stage of evaporative cooling, we apply the optical pumping [26] to create balanced two- or four-component mixtures of ^{173}Yb (See S.1 in the Supplemental Material (SM) [27] for the details of the optical pumping schemes). The spin distribution after optical pumping is measured by an Optical Stern-Gerlach (OSG) technique [26], where we apply the spin-dependent gradient by an circularly polarized laser beam with a Gaussian profile. After loading the two- or four-component Fermi gas into a strongly dimerized lattice, where all beams are simultaneously ramped in 150 ms with a spline-shaped

laser intensity, we detect an antiferromagnetic spin correlation with the sequence as shown in Fig.2 (a), similar to Ref.[3]. In the first part of the detection sequence, we freeze out the atomic motion by applying a two-step ramp of $s_{\text{L}} = [(20, 20.8), 48, 48] \rightarrow [(25, 20.8), 80, 100] \rightarrow [(25, 100), 80, 100]$. The first ramp and the second ramp take 0.5 ms and 10 ms, respectively. This lattice ramp also removes the contribution of the admixture of double occupancies in the ground-state singlet (S.2 in SM [27]). Then, we apply a spin-dependent gradient by a fictitious magnetic field of light, similar to the OSG beam. This gradient creates an energy difference Δ for atoms with different spins on neighboring sites and drives coherent oscillation between the singlet$= (|\sigma_1, \sigma_2\rangle - |\sigma_2, \sigma_1\rangle)/\sqrt{2}$ and triplet $|t_0\rangle = (|\sigma_1, \sigma_2\rangle + |\sigma_2, \sigma_1\rangle)/\sqrt{2}$ states at a frequency of $\Delta/\hbar$ [23], where σ_i ($i = 1, 2$) denotes a spin component. For a four-component mixture, we use a linearly polarized gradient beam, with which the STOs have the same frequency for the 4 spin pairs of $(m_F = 5/2, 1/2), (5/2, -1/2), (-5/2, 1/2)$, and $(-5/2, -1/2)$, but do not occur for the 2 spin pairs of $(5/2, -5/2)$ and $(1/2, -1/2)$ (S.3 in SM [27]). After a certain oscillation time, we remove the gradient and merge the dimers into single sites by ramping the lattice po-

tential down to $s_{\mathrm{L}} = [(25,0), 80, 100]$ in 1 ms. Due to a fermion anticommutation relation and symmetry of the two-particle wave function, the singlet state on adjacent sites evolves to a doubly occupied site with both atoms in the lowest band, while the triplet state transforms into a state with one atom in the lowest band and the other in the first excited band. The fraction of atoms forming double occupancies in the lowest band is detected by a photoassociation (PA) technique [21, 28, 29]. The PA process enables us to convert all atoms forming double occupancies in the lowest band into electronically excited molecules that rapidly escape from the trap, whereas the state with one atom in the lowest band and the other in the first excited band is not converted due to its odd-parity of relative spatial wave functions [30]. Therefore, the loss of atoms corresponds to the number of atoms forming the singlet state in the initial dimerized lattice. We note that the symmetric and antisymmetric states= $(|\sigma_1, 0\rangle \pm |0, \sigma_1\rangle)/\sqrt{2}$ also exist, especially in the trap edge, but they evolve to the state with one atom per site after merging the dimer, which is not detected by a PA. The PA laser is detuned by -812.26 MHz from the $^{1}S_0 \leftrightarrow ^{3}P_1(F' = 7/2)$ transition and has sufficient intensity to finish removing double occupancies within 0.5 ms irradiation.

Figure 2 (b) shows the typical STO of SU(4) spins in a strongly dimerized lattice. A clear oscillation is visible. The damping of oscillation is caused by the spatial inhomogeneity of the fictitious magnetic gradient and the photon scattering from the gradient beam (S.4 in SM [27]). This oscillation reveals an excess number of singlets compared to triplets, corresponding to an antiferromagnetic correlation on neighboring sites. An STO signal is also observed for an SU(2) system. We fit the data with the empirical function

$$F(t_{\mathrm{STO}}) = -a\, e^{-t_{\mathrm{STO}}/\tau} \cos\left(2\pi f t_{\mathrm{STO}}\right) + b, \qquad (5)$$

where a, b, τ, f are fitting parameters. Along with the data of STO, we measure the total atom number in the optical lattice without applying the PA laser, N. We quantify this correlation by the normalized STO amplitude A and singlet fractions p_s:

$$A = \begin{cases} 2a/N & \text{for SU(2)} \\ 3a/N & \text{for SU(4)} \end{cases} \qquad (6)$$

$$p_s = 1 - \frac{b-a}{N}. \qquad (7)$$

We note that the extracted $N - b - a$ exactly corresponds to the actual atom number in the triplet state $|t_0\rangle$ for SU(2) spins, but that is not the case for SU(4) spins because a coherent oscillation does not occur for the spin pairs of $(m_F = 1/2, -1/2)$ and $(5/2, -5/2)$. To take this effect into consideration, we compensate the measured STO amplitude by multiplying 3/2 for SU(4) case as in Eq.(6).
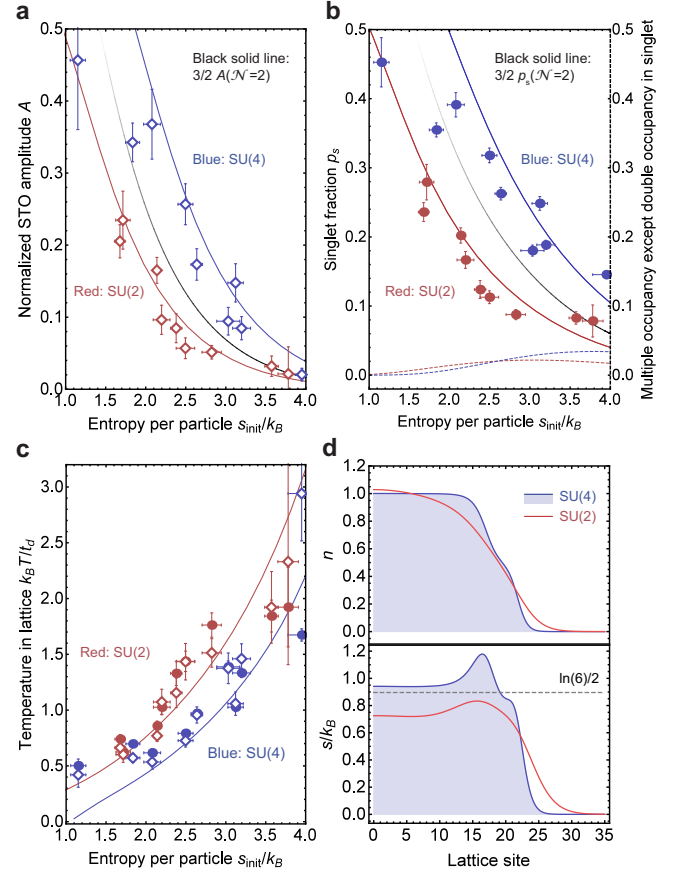

FIG. 3. (a) Normalized STO amplitude and (b) singlet fraction of SU(2) and SU(4) Fermi gases in the strongly dimerized lattice of $t_{\mathrm{d}}/t = 27$. The dependence on the initial entropy in the harmonic trap is shown. The solid line is a theoretical curve that assumes adiabatic loading into the lattice. The dotted line in (b) is the numerically calculated multiple occupancy except the double occupancy in the ground-state singlet wave function. The vertical error bars include the fitting errors in the STO measurement and the standard deviation of the total atom number N. The horizontal error bars show the standard deviation of the 10 independent temperature measurements. (c) Temperature of SU(2) and SU(4) Fermi gases in the lattice. The empty diamond and filled circle are the experimental data estimated from (a) and (b), respectively. Solid line is a theoretical curve. (d) Calculated density (top) and entropy distribution (bottom) at the initial entropy per particle $s_{\mathrm{init}}/k_{\mathrm{B}} = 1.5$ for SU(2) and SU(4) cases. The maximum singlet entropy per site $\ln(6)/2$ for SU(4) is indicated by the gray dashed line.

To reveal the influence of spin degrees of freedom on the magnetic correlations, we investigate A and p_s for various initial entropies in the harmonic trap. Figure 3 (a) and (b) show the results comparing SU(2) and SU(4) systems in a strongly dimerized lattice. The initial temperature in the harmonic trap is obtained by performing the Thomas-Fermi fitting to the 10 independent momentum distributions and the initial en-

tropy s_{init} is calculated from the T/T_{F} using the formula for a non-interacting Fermi gas, where T_{F} is the Fermi temperature. The STO data are taken for the atom number of $N = 3.2 \times 10^4$ and the trap frequencies of $(\omega_x, \omega_y, \omega_z)/2\pi = (158.3, 48.6, 141.8)$ Hz, where the filling n, i.e., the number of the particle per site, amounts to $n = 1$ around the trap center (Fig.3 (d)). The solid lines are the result of the atomic limit calculation based on the SU($\mathcal{N}$) FHM in Eq.(1), assuming the local density approximation (S.5 in SM [27]). The normalized STO amplitude and the absolute singlet fraction decrease for larger entropies, as triplet states become thermally populated. A clear and striking difference between SU(2) and SU(4) systems is visible: the antiferromagnetic correlation is enhanced in the SU(4) system compared to SU(2) for the same initial entropy. There are two effects at play. One is the difference of the fraction of singlet configurations among all possible states. The other is the thermodynamic cooling effect related to spin entropy. To discuss these effects, we consider two atoms with SU($\mathcal{N}$) spin symmetry in an isolated dimer, neglecting double occupancies. At the zero temperature, the singlet probability is $p_{\mathrm{s}}(\mathcal{N}) = 1$ regardless of $\mathcal{N}$ because the singlet is the ground state. On the other hand, at the infinite temperature, the singlet probability is $p_{\mathrm{s}}(\mathcal{N}) = W(\mathcal{N})/\mathcal{N}^2$ because the probability is determined by the number of the singlet configurations $W(\mathcal{N}) = {}_{\mathcal{N}}C_2$. For SU(2) and SU(4), the ratio of the singlet probabilities at the same temperature becomes

$$p_{\mathrm{s}}(4)/p_{\mathrm{s}}(2) = \begin{cases} 1 & \text{for } T = 0 \\ 3/2 & \text{for } T = \infty. \end{cases} \quad (8)$$

Because this ratio monotonically decreases from $3/2$ to 1 as the temperature gets lowered, $p_{\mathrm{s}}(2) < p_{\mathrm{s}}(4) < 3/2 p_{\mathrm{s}}(2)$ holds for a finite temperature. The same inequality is true for $A(4)$ and $A(2)$. The black solid lines in Fig.3 (a) and (b) indicate $3/2 p_{\mathrm{s}}(2)$ and $3/2 A(2)$, which should give the upper limit for $p_{\mathrm{s}}(4)$ and $A(4)$ at the same temperature. Most of the observed SU(4) data are above the black lines at the same initial entropy. This means that the temperature of SU(4) is lower than that of SU(2), which is ensured from Fig.3 (c). This behavior can be understood as follows. Entropy per site of the singlet ground states is given by $\ln(W(\mathcal{N}))/2$. In contrast to the zero-entropy ground state of SU(2) system, the SU(4) ground state has a residual entropy of $\ln(6)/2 = 0.9$. Therefore, the initial temperature required for spins to form the singlet is increased in the SU(4) system compared to SU(2). This is closely related to the Pomeranchuk effect [31] enhanced by large spin degrees of freedom, which was already demonstrated in the paramagnetic SU(6) fermionic Mott-insulator [21]. In this work, it is clearly shown that cooling with large SU($\mathcal{N}$) spin can be applied even in the regime of quantum magnetism. We note that in a trapped system, entropy
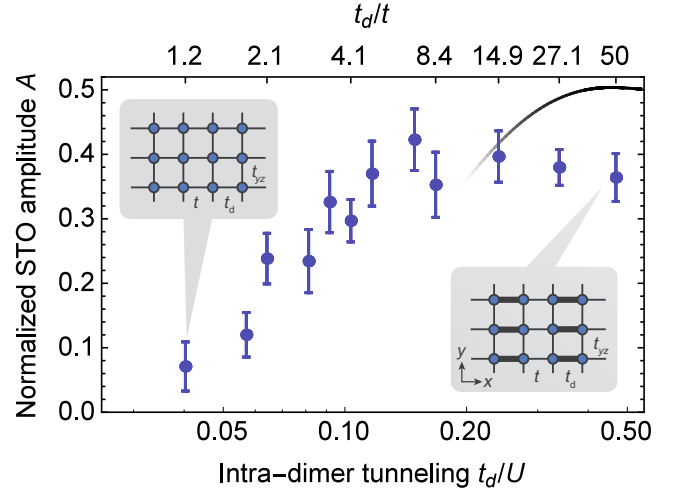

FIG. 4. Normalized STO amplitude for the SU(4) Fermi gas versus the intra-dimer tunneling. The bottom axis is shown in a logarithmic scale. The black solid curve is the prediction in the atomic limit for an entropy per particle of $s/k_{\mathrm{B}} = 1.9$ under the assumption of the adiabatic loading into the lattice, and is shown down to $t_{\mathrm{d}}/t = 10$. For the entire data, the on-site interaction is fixed to $U/h = 3.0$ kHz, while t changes from $t/h = 28.0$ Hz to 100 Hz, and t_{yz}/t from 1.7 to 1.0.

is stored in a low-density metallic state near the edge of the atomic cloud and singlet states at the trap center survive for higher total entropy as in Fig.3 (d). The data in Fig.3 (a) and (b), especially at low initial entropies, show the discrepancy with the theory. This might be caused by several reasons including some non-adiabaticity in the lattice loading or an imperfect efficiency on the PA (S.6 in SM [27]). From middle to high initial entropies, the measured singlet fraction is slightly overestimated because the multiply occupied states except the ground-state singlet are thermally populated at the initial lattice depth and detected by PA after merging.

Finally, we investigate the dependence of the normalized STO amplitude on the intra-dimer tunneling t_{d}. Figure 4 shows the result with the SU(4) Fermi gas. The solid line is the theoretical curve shown only for $t_{\mathrm{d}}/t = 10$ and higher. Below this value the atomic limit calculation starts to be invalid. As t_{d} decreases, the STO amplitude gets smaller because the excitation energy to the triplet state, which is determined by the exchange energy $-U/2 + \sqrt{16t_{\mathrm{d}}^2 + U^2}/2$, is lowered. Our experimental data show such a tendency and indicate the possibility that the nearest-neighbor antiferromagnetic correlation still remains slightly even in the isotropic lattice. In terms of the entropy, the rough criterion for the onset of the nearest-neighbor spin correlation in the lattice is $s/k_{\mathrm{B}} = \ln(\mathcal{N})$ [32], which amounts to $\ln(\mathcal{N} = 4) = 1.38$ for SU(4) system. Even though the average entropy in our trapped system is 1.9 in Fig.4, the lower entropy is

achieved at the trap center. The atoms around such a region are considered to contribute to the possible nearest-neighbor spin correlation in the isotropic lattice.

In conclusion, we have studied the important role of the spin degrees of freedom on the antiferromagnetic correlation in a strongly dimerized lattice by comparing the SU(2) and SU(4) systems. We observed the enhanced antiferromagnetic correlation in SU(4) due to the Pomeranchuk effect. Further cooling can be expected for a larger spin system such as SU(6), which ^{173}Yb possesses. The bottleneck for experiments with higher spin system is the detection technique: if we applied the scheme performed here to SU(6) system of ^{173}Yb, we would suffer from the multiple STO frequencies. We expect that combining SU($\mathcal{N} > 2$) Fermi gas with more complex lattice geometry like a plaquette, which has been already implemented with optical lattices [33, 34], will open up the door to the interesting magnetic order [35, 36].

---

* Electronic address: hideki_ozawa@scphys.kyoto-u.ac.jp

[1] A. Auerbach, *Interacting Electrons and Quantum Magnetism*, Graduate Texts in Contemporary Physics (Springer New York, 2012).

[2] I. Bloch, J. Dalibard, and S. Nascimbene, Nature Phys **8**, 267 (2012).

[3] D. Greif, T. Uehlinger, G. Jotzu, L. Tarruell, and T. Esslinger, Science **340**, 1307 (2013).

[4] D. Greif, G. Jotzu, M. Messer, R. Desbuquois, and T. Esslinger, Phys. Rev. Lett. **115**, 260401 (2015).

[5] R. A. Hart, P. M. Duarte, T.-L. Yang, X. Liu, T. Paiva, E. Khatami, R. T. Scalettar, N. Trivedi, D. A. Huse, and R. G. Hulet, Nature **519**, 211 (2015).

[6] M. Boll, T. A. Hilker, G. Salomon, A. Omran, J. Nespolo, L. Pollet, I. Bloch, and C. Gross, Science **353**, 1257 (2016).

[7] M. F. Parsons, A. Mazurenko, C. S. Chiu, G. Ji, D. Greif, and M. Greiner, Science **353**, 1253 (2016).

[8] L. W. Cheuk, M. A. Nichols, K. R. Lawrence, M. Okan, H. Zhang, E. Khatami, N. Trivedi, T. Paiva, M. Rigol, and M. W. Zwierlein, Science **353**, 1260 (2016).

[9] A. Mazurenko, C. S. Chiu, G. Ji, M. F. Parsons, M. Kanász-Nagy, R. Schmidt, F. Grusdt, E. Demler, D. Greif, and M. Greiner, Nature **545**, 462 (2017).

[10] P. T. Brown, D. Mitra, E. Guardado-Sanchez, P. Schauß, S. S. Kondov, E. Khatami, T. Paiva, N. Trivedi, D. A. Huse, and W. S. Bakr, Science **357**, 1385 (2017).

[11] C. Honerkamp and W. Hofstetter, Phys. Rev. Lett. **92**, 170403 (2004).

[12] R. W. Cherng, G. Refael, and E. Demler, Phys. Rev. Lett. **99**, 130406 (2007).

[13] M. Hermele, V. Gurarie, and A. M. Rey, Phys. Rev. Lett. **103**, 135301 (2009).

[14] A. V. Gorshkov, M. Hermele, V. Gurarie, C. Xu, P. S. Julienne, J. Ye, P. Zoller, E. Demler, M. D. Lukin, and A. M. Rey, Nature Physics **6**, 289 (2010).

[15] S. Capponi, P. Lecheminant, and K. Totsuka, Annals of Physics **367**, 50 (2016).

[16] T. Fukuhara, Y. Takasu, M. Kumakura, and Y. Takahashi, Phys. Rev. Lett. **98**, 030401 (2007).

[17] B. J. DeSalvo, M. Yan, P. G. Mickelson, Y. N. Martinez de Escobar, and T. C. Killian, Phys. Rev. Lett. **105**, 030402 (2010).

[18] M. K. Tey, S. Stellmer, R. Grimm, and F. Schreck, Phys. Rev. A **82**, 011608 (2010).

[19] C. Wu, J.-p. Hu, and S.-c. Zhang, Phys. Rev. Lett. **91**, 186402 (2003).

[20] M. A. Cazalilla, A. F. Ho, and M. Ueda, New Journal of Physics **11**, 103033 (2009).

[21] S. Taie, R. Yamazaki, S. Sugawa, and Y. Takahashi, Nature Physics **8**, 825 (2012).

[22] C. Hofrichter, L. Riegger, F. Scazza, M. Höfer, D. R. Fernandes, I. Bloch, and S. Fölling, Phys. Rev. X **6**, 021030 (2016).

[23] S. Trotzky, Y.-A. Chen, U. Schnorrberger, P. Cheinet, and I. Bloch, Physical Review Letters **105**, 265303 (2010).

[24] D.-S. Lühmann, O. Jürgensen, M. Weinberg, J. Simonet, P. Soltan-Panahi, and K. Sengstock, Phys. Rev. A **90**, 013614 (2014).

[25] S. Trotzky, P. Cheinet, S. Fölling, M. Feld, U. Schnorrberger, A. M. Rey, A. Polkovnikov, E. A. Demler, M. D. Lukin, and I. Bloch, Science **319**, 295 (2008).

[26] S. Taie, Y. Takasu, S. Sugawa, R. Yamazaki, T. Tsujimoto, R. Murakami, and Y. Takahashi, Phys. Rev. Lett. **105**, 190401 (2010).

[27] See Supplemental Material at [url] for the theoretical and experimental details, which includes Refs. [3, 37–39].

[28] S. Sugawa, K. Inaba, S. Taie, R. Yamazaki, M. Yamashita, and Y. Takahashi, Nature Phys. **7**, 642 (2011).

[29] T. Rom, T. Best, O. Mandel, A. Widera, M. Greiner, T. W. Hänsch, and I. Bloch, Phys. Rev. Lett. **93**, 073002 (2004).

[30] K. M. Jones, E. Tiesinga, P. D. Lett, and P. S. Julienne, Rev. Mod. Phys. **78**, 483 (2006).

[31] R. C. Richardson, Rev. Mod. Phys. **69**, 683 (1997).

[32] L. Messio and F. Mila, Physical Review Letters **109**, 205306 (2012).

[33] H.-N. Dai, B. Yang, A. Reingruber, H. Sun, X.-F. Xu, Y.-A. Chen, Z.-S. Yuan, and J.-W. Pan, Nature Physics **13**, 1195 (2017).

[34] S. Nascimbène, Y.-A. Chen, M. Atala, M. Aidelsburger, S. Trotzky, B. Paredes, and I. Bloch, Phys. Rev. Lett. **108**, 205301 (2012).

[35] N. Read and S. Sachdev, Phys. Rev. Lett. **62**, 1694 (1989).

[36] Y. Q. Li, M. Ma, D. N. Shi, and F. C. Zhang, Phys. Rev. Lett. **81**, 3527 (1998).

[37] H. J. Metcalf and P. van der Straten, *Springer-Verlag Berlin Heidelberg*, Vol. 13 (1999) p. 323.

[38] C. Cohen-Tannoudji, "Atom-Photon Interactions: Basic Processes and Applications" (1993).

[39] S. G. Porsev, Y. G. Rakhlina, and M. G. Kozlov, Phys. Rev. A **60**, 2781 (1999).